Journal of
Materials Chemistry C

PAPER

View Article Online
View Journal

Cite this: DOI: 10.1039/c6tc01088a

Influence of heteroatoms on the charge mobility of anthracene derivatives†

Lijia Yan,[a] Yang Zhao,[a] Hongtao Yu,[a] Zhao Hu,[b] Yaowu He,[b] Aiyuan Li,[b] Osamu Goto,[b] Chaoyi Yan,[b] Ting Chen,[a] Runfeng Chen,[a] Yueh-Lin Loo,[c] Dmitrii F. Perepichka,[d] Hong Meng*[ab] and Wei Huang*[a]

Received 14th March 2016,
Accepted 18th March 2016

DOI: 10.1039/c6tc01088a

www.rsc.org/MaterialsC

The introduction of polarizable heteroatom, such as O, and S, attached peripheral side chains of conjugated moieties such as polyacenes has not been systematically investigated. To study such effects, and to explore semiconductors with both high charge mobility and luminescence properties, we present a comparative systematic study of heteroatom effects on the conduction of organic semiconductors in a representative series of new organic semiconductors based on the blue phenyl-anthracene molecule core. Elucidated by the single-crystal X-ray analysis, thin film XRD and AFM measurements, a correlation between the molecular structure variation, film ordering, and charge mobility has been established. Quantum chemistry calculations combined with the Marcus–Hush electron transfer theory interpret the transport parameters. The anisotropic transport properties of these compounds were suggested by the DFT predictions and the high hole mobility in BEPAnt and BOPAnt is contributed mainly by the parallel packing of these compounds with the highest $\|\mu_h$; these results are in good agreement with the experimental observations. Heteroatoms are demonstrated to influence the charge mobility dramatically. Our systematic investigation will provide valuable guidance for a judicious material design of semiconductors for OTFT applications.

Introduction

The possibility of introducing various heteroatoms (nitrogen, oxygen, sulfur, *etc.*) in organic compounds creates an infinite variety of organic materials compared with inorganic counterparts.[1–4] This feature enables organic molecules to form semiconducting materials with almost limitless varieties in molecular structures and resulting properties, such as luminescence, p-, n- or ambipolar charge transport, photoconductivity, thermoelectricity, and even superconductivity.[5] These prominent properties enable the organic semiconductors to be successfully applied in various organic electronic devices, including organic light emitting diodes (OLEDs),[6] organic thin film transistors (OTFTs),[7] and organic photovoltaics (OPVs).[8,9] Combining several of such properties in a single material could lead to even more interesting applications. For example, organic light emitting transistors (OLETs),[10,11] with the dual functionality of light emission and current switching amplification, have been proposed to simplify active matrix displays and develop electrically driven organic lasers.[12] Organic semiconductors with high charge mobility and luminescence are highly desired for the applications.[11] However, achieving high charge mobility requires crystalline materials with strong π-interactions and thus more conjugated and flat structures. Meanwhile obtaining highly emissive organic solids typically demands suppressing the π-interactions in order to avoid exciton quenching.[13] Thus it is difficult to achieve high charge mobility and good luminescence in the same materials, since they have contradictory structural requirements.[14] This represents a dilemma in the design of the OLET materials and the design rules for such materials are presently unclear. A particular problem presents for blue light emitting transistors, where less π-extended molecules with a larger bandgap are required. It is well known that many π-extended acene compounds with their flat and conjugated molecular structures demonstrated high charge mobility.[15] Numerous other organic semiconductors, such as dibenzothiophene thiophene and its derivatives, have also been investigated and some semiconductors with mobility over 17 $cm^2 V^{-1} s^{-1}$ have been recently reported.[16] However, all these semiconductors showed low or no luminescence properties, excluding their applications in OLET devices.

[a] Key Laboratory of Flexible Electronics (KLOFE) & Institute of Advanced Materials (IAM), Jiangsu National Synergetic Innovation Center for Advanced Materials (SICAM), Nanjing Tech University (Nanjing Tech), 30 South Puzhu Road, Nanjing 211816, China. E-mail: iamhmeng@njtech.edu.cn, wei-huang@njtech.edu.cn
[b] School of Advanced Materials, Peking University Shenzhen Graduate School, Peking University, Shenzhen, 518055, China
[c] Department of Chemical and Biological Engineering, Princeton University, A215 Engineering Quadrangle, Princeton, NJ 08544, USA
[d] Department of Chemistry and Center for Self-Assembled Chemical Structures, McGill University, 801 Sherbrooke Street West, Montreal, H3A 0B8, QC, Canada

† Electronic supplementary information (ESI) available: Experimental details for synthesis of BOPAnt, BSPAnt and BEPAnt, their characterization, and single crystal CIF data; OFET device fabrication details. CCDC 1442077–1442079. For ESI and crystallographic data in CIF or other electronic format see DOI: 10.1039/c6tc01088a

Compared with pentacene and tetracene molecules, which suffer from hard peripheral functionalization, instability, and low luminescence properties in the solid state, anthracene shows more synthetic versatility, better core stability and possesses much higher blue fluorescence properties.[17] In fact, anthracene derivatives have been widely explored in recent years, and charge mobilities up to 10 $cm^2\ V^{-1}\ s^{-1}$ have been reported.[18–20] These compounds are easily synthesized and can be modified with a variety of substituents.[21] Motivated by the fact that the heteroatom substitution of organic molecules could induce different optical and electrochemical performances, and combining the unique properties of anthracene derivatives, we have decided to explore the possiblity to fine-tune their optical and electronic behaviors by introducing heteroatoms,[22,23] with a hope to achieve high charge mobility materials while maintaining blue fluorescence properties. In this communication, we synthesize and study three related oligomers using a 2,6-diphenylanthracene core and C-, O-, and S-bridged alkyl chain substituents, to establish the relationship between the electronic properties of the molecules and their structures. To the best of our knowledge, the influence of the elements on the peripheral side chain of the molecular semiconductor core has not yet been systematically elucidated.

Experimental

Synthesis

2,6-Dibromoanthracene (3.36 g, 10 mmol), the respected substituted benzenyl boronic acid (25 mmol) and tetrakis(triphenylphosphine)Pd(PPh_3)$_4$ (0.231 g, 0.2 mmol) were added to a 350 mL high-pressure reaction bottle filled with toluene (70 mL). A nitrogen degassed aqueous solution of 2 M Na_2CO_3 (33 mL, 66 mmol) was added and stirred for 10 min under nitrogen. Then a phase transfer agent cetyltrimethylammonium bromide (1 mL) was added, and the mixture was heated at 85 °C for 36 h. The resulting solids were collected by filtration, washed with methanol, diluted hydrochloric acid aqueous solution and acetone, respectively. The obtained crude product was collected by filtration. It was further purified using a 3-zone furnace under high vacuum two times to give the pure crystal compounds. BOPAnt: MALDI-TOF-MS m/z: 391.16; anal. calculated for $C_{28}H_{22}O_2$ (M_w: 390.16): C, 85.13; H, 5.68. Found: C, 85.86; H, 5.52. BSPAnt: MALDI-TOF-MS m/z: 423.12; anal. calculated for $C_{28}H_{22}S_2$ (M_w: 422.12) anal. calculated for $C_{28}H_{22}S_2$: C, 79.58; H, 5.25; S, 15.17. Found: C, 79.86; H, 5.34; S, 14.97. BEPAnt: MALDI-TOF-MS m/z: 387.21; calculated for $C_{30}H_{26}$: 386.20 anal. calculated for $C_{30}H_{26}$: C, 93.22; H, 6.78. Found: C, 93.17; H, 6.65.

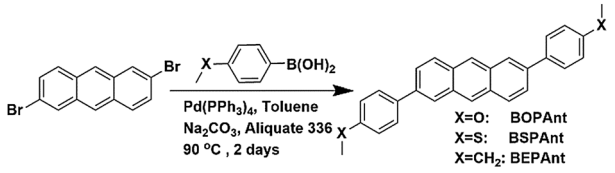

Scheme 1 Synthetic route to BOPAnt, BSPAnt and BEPAnt.

Device fabrication and measurement

Top contact organic field-effect transistors (OTFTs) were constructed on heavily doped n-type silicon wafers with 200 nm of thermally grown silicon dioxide, which was cleaned using piranha solution. The n-Si layer was used as the gate electrode, and the silicon dioxide layer served as the gate dielectric which has been modified using octadecyltrichlorosilane (OTS). The semiconductor layers (38 nm) were deposited on the top of the OTS-modified SiO_2 surface for device fabrication and GCE (Φ = 3 mm) for CV measurements by the vapour deposited process (Fig. S1, ESI†). Gold source and drain electrodes (58 nm) were vapour-deposited at 2×10^{-4} Torr through shadow mask in the vacuum deposition chamber. Devices were fabricated with typical channel lengths (L) of 38, 58, 78, and 98 μm and channel widths (W) of 380, 580, 780, and 980 μm, respectively.

The electrical characterization of the fabricated OTFTs was carried out in air using an Agilent 1500B parameter analyzer on a probe stage. The carrier mobility (μ) was calculated from the data in the saturated regime according to the equation $I_{SD} = \mu C_i(W/2L)\ (V_G - V_T)^2$, where I_{SD} is the drain current, μ is the carrier mobility, C_i is the capacitance per unit area of the gate dielectric layer, W and L are the channel width and length, respectively, and V_G and V_T are the gate voltage and threshold voltage, respectively.

Molecule modelling

DFT calculations were performed using Gaussian 09 program. The geometries of the ground states (S_0) and the charged states were fully optimized with Becke's three-parameter exchange function along with Lee Yang Parr's correlation function (B3LYP) using 6-31G(d) basis sets. Harmonic vibrational frequency analysis was performed to confirm the optimized stationary points as the real minima on respective potential energy surfaces.

Results and discussion

Scheme 1 shows the synthetic routes of BXPAnt, where X represents CH_2, O or S. The compounds were synthesized by Suzuki coupling of 2,6-dibromo-anthracene with the corresponding substituted phenylboronic acid, and then purified three times by gradient sublimation. Due to their low solubility, the synthesized semiconductors were characterized by high-resolution mass spectrometry, elemental analysis, and single crystal analysis. Thermogravimetric analysis (TGA) showed the thermal stability up to 350 °C for BOPAnt and BSPAnt, and up to 300 °C for BEPAnt, respectively (Fig. S2a, ESI†). Note that only BSPAnt shows the signs of chemical decomposition, while the complete mass loss of BEPAnt and BOPAnt suggests their clean sublimation at these temperatures. Differential scanning calorimetry (DSC) shows reversible melting and recrystallization for BOPAnt and BEPAnt, but not for BSPAnt, which decomposes after melting at 370 °C (Fig. S2b, ESI†).

Single crystal X-ray analyses of three anthracene derivatives reveal a typical herringbone packing structure with two-dimensional short contacts in the bulk single-crystal phase

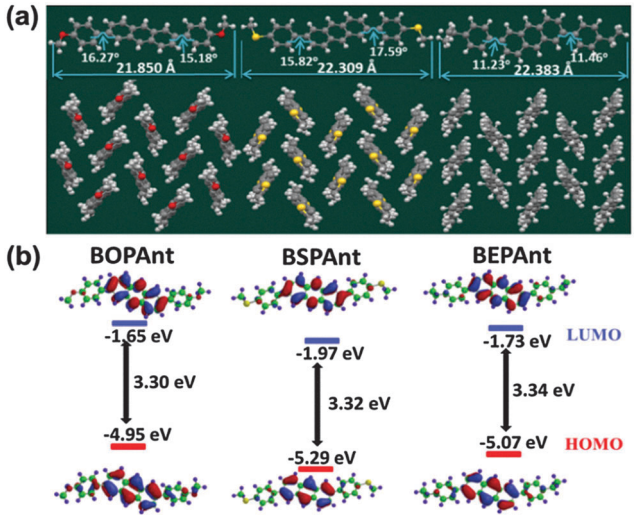

Fig. 1 (a) Molecular length, herringbone packing and single crystal structures of BOPAnt, BSPAnt and BEPAnt (from left to right, respectively). (b) The frontier molecular orbitals for BOPAnt, BSPAnt and BEPAnt at the B3LYP/6-31G* level.

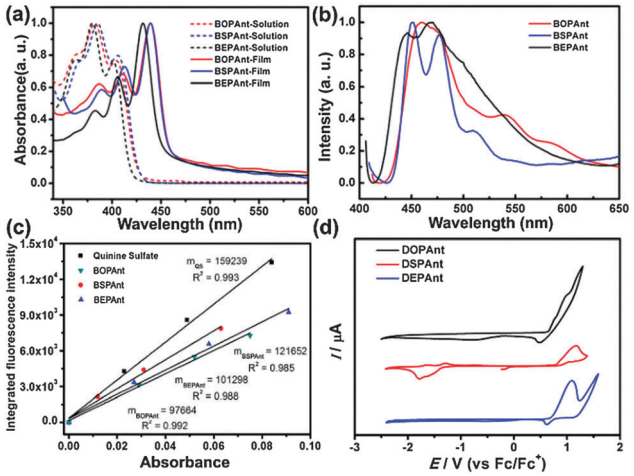

Fig. 2 (a) UV-vis spectra of BOPAnt, BSPAnt and BEPAnt in chloroform solution (dashed line) and in thin films (solid line); (b) PL spectra of the semiconductors in thin films; (c) quantum yields of BOPAnt, BSPAnt and BEPAnt (quinine sulfate as the standard); (d) cyclic voltammetry of BOPAnt, BSPAnt and BEPAnt thin film on GCE (Φ = 3 mm) in CH_2Cl_2/TBAPF$_6$ solution (potential *vs.* ferrocene).

(Fig. 1 and Table S1, ESI†). We note that most high mobility organic semiconductor materials tend to take a similar herringbone packing.[16–19] The molecules are almost planar which is essential for the intramolecular conjugation and intermolecular stacking. The two torsion angles between the anthracene core and the substituted phenyl groups are 16.3° and 15.2° for BOPAnt, 17.6° and 15.8° for BSPAnt and 11.2° and 11.5° for BEPAnt (Fig. 1a). The increased planarization of the molecule with stronger intermolecular packing is expected to lead to higher charge mobility in semiconducting devices. Density functional theory (DFT) calculations on the three compounds were performed using the B3LYP function and the 6-31G* basis set as implemented in Spartan'14 program (Fig. 1b).[24] Both HOMO and LUMO energy levels are localized on the anthracene core, despite the different substituents.

The optical and electrochemical properties of the three compounds were investigated in chloroform and in thin films. The normalized absorption spectra of BOPAnt, BSPAnt, BEPAnt in thin films and in solution exhibited pronounced finger-like vibrational splitting peaks (Fig. 2a). These major absorption bands in the range of 330–460 nm can be ascribed to the π–π* transition of the diphenyl anthracene core and only a slight bathochromic shift was observed for methoxy and methylsulfanyl derivatives, likely due to the conjugation of the heteroatom lone pair.[25,26] The UV-vis spectra of vacuum-deposited thin films of BOPAnt, BSPAnt and BEPAnt reveal a *ca.* 0.04 eV red-shift of absorption compared to solution (Fig. 2a). The optical band gaps estimated from the absorption edges of the thin-film spectra are 2.76 eV, 2.72 eV, and 2.77 eV for BOPAnt, BSPAnt, and BEPAnt, respectively. In photoluminescence (PL) spectra (Fig. 2b), all compounds exhibited strong blue fluorescence emission both in solution and in the thin films. The fluorescence quantum efficiency (QE) was in the range of 42–50% (Fig. 2c).

To assess the ionization potentials and further elucidate the influence of the heteroatoms, cyclic voltammetry (CV) measurements on the vacuum deposited thin films of the semiconductors were tested.[27] The reduction behaviour of the thin films was irreversible and thus we only estimated their HOMO energies (Fig. 2d). All compounds BOPAnt, BSPAnt and BEPAnt showed quasi-reversible oxidation waves, with the onset of the first oxidation potentials of 0.65 V, 0.80 V, and 0.69 V (*vs.* Fc/Fc$^+$), respectively. These values correspond to HOMO energy levels of −5.45 eV, −5.60 eV and −5.49 eV. The HOMO energy levels are in good agreement with calculations, and are slightly lower than that for pentacene (5.0 eV).[28] The electrochemical properties along with derived orbital energies are summarized in Table 1.

All three compounds yield uniform thin films *via* thermal evaporation (evaporation source temperatures are below 300 °C). Top contact OTFT devices were fabricated with 50 nm semiconductor films deposited onto an octyltrichlorosilane (OTS) pre-treated SiO_2 (200 nm)/n-doped Si substrate. The heavily doped n-type Si layer was used as the gate electrode and the gold layer (60 nm) was evaporated through a shadow mask to form the source and drain electrodes with three channel dimensions: of 38 μm × 380 μm, 58 μm × 580 μm and 78 μm × 780 μm. The devices were measured under ambient conditions. Fig. 3 shows well defined linear-regime and saturation-regime output characteristics of the BEPAnt semiconductor OTFT device. Table 2 lists the charge mobility data of all the semiconductors along with molecule modelling data for comparison. The detailed device information can be found in Fig. 3. The BEPAnt based devices showed the highest performance (μ^+ = 3.72 cm^2 V^{-1} s^{-1}), which is followed closely by BOPAnt (2.96 cm^2 V^{-1} s^{-1}), while the mobility of BSPAnt (0.12 cm^2 V^{-1} s^{-1}) based devices is over one order of magnitude lower. All the semiconductors showed higher charge mobility when fabricated at higher substrate deposition temperature. In all cases, the on/off ratios of all

Table 1 Optical and electrochemical properties of diphenylanthracene semiconductors

Semi-conductor	λ_{max}^{abs} sol[a] (nm)	λ_{max}^{abs} film[b] (nm)	λ_{max}^{pl} film[c] (nm)	PLQY[d]	$E_g^{opt\,e}$ (eV)	$E_{ox}^{onset\,f}$ (V)	$E_{HOMO}{}^{g}$ (eV)	$E_{LUMO}{}^{h}$ (eV)	$E_{HOMO}^{calcd\,i}$ (eV)	$E_{LUMO}^{calcd\,i}$ (eV)
BOPAnt	385	439	460	0.42	−2.70	0.65	−5.45	−2.76	−4.95	−1.65
BSPAnt	385	439	450	0.52	−2.71	0.80	−5.60	−2.72	−5.29	−1.97
BEPAnt	380	432	470	0.43	−2.74	0.69	−5.49	−2.77	−5.07	−1.73

[a] Solution absorption spectra (1×10^{-5} M in chloroform). [b] Thin film absorption spectra of the pristine film cast from evaporation of the solid material. [c] Solution fluorescence spectra (1×10^{-5} M in chloroform). [d] Fluorescence quantum efficiency. [e] Optical energy gap estimated from the absorption edge of the thin film. [f] Electrochemically determined *vs.* Fc/Fc$^+$. [g] $E_{HOMO} = -(E_{ox}^{onset} + 4.80)$. [h] Values in the parentheses calculated according to: $E_{LUMO} = E_g^{opt} + E_{HOMO}$. [i] Calculated by DFT (B3LYP/6-31G* level).

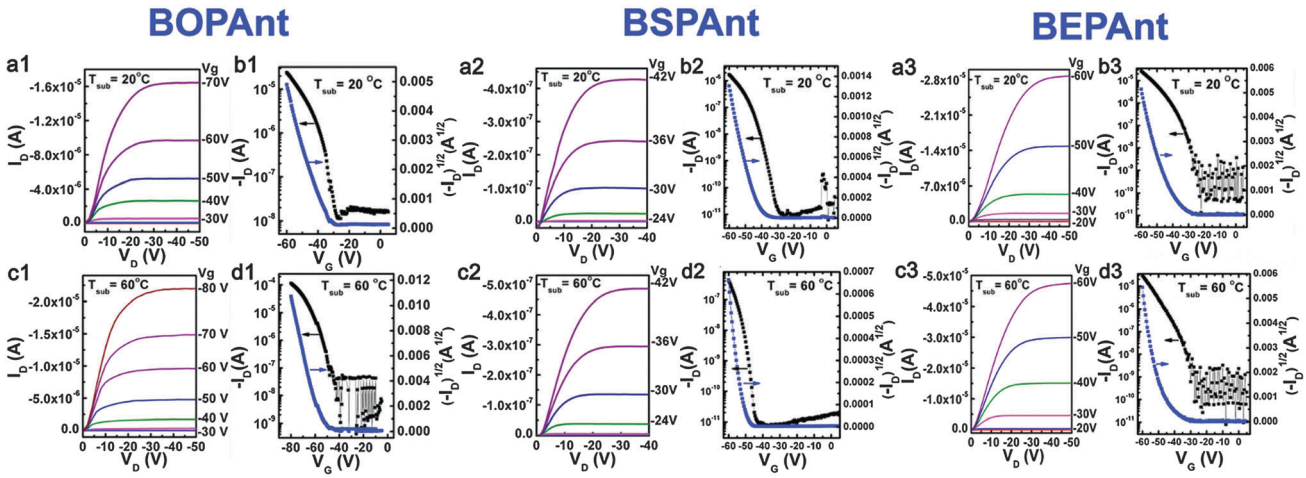

Fig. 3 Transfer and output plots of OTFTs of BOPAnt, BSPAnt and BEPAnt films grown on an OTS-coated substrate at T_{sub} = 20 °C and T_{sub} = 60 °C: (a1–a3) and (c1–c3) output plot; (b1–b3) and (d1–d3) transfer plot.

OFETs are very high, which we attribute to the large band gap and excellent stabilities of these semiconductors. The achieved mobilities are much higher than those of bench-mark pure pentacene devices (0.5–0.6 cm^2 V^{-1} s^{-1}) fabricated under the same conditions. We noticed that the high threshold voltages exist in all our devices. This is due to the charge trap states which limit the charge injection, and thus the intrinsic mobility should be higher than measured.[29] XRD data reveal highly crystalline films for all studied derivatives. Most of the major peaks in the thin-film XRD patterns can be indexed according to the crystal structures extracted from single-crystal X-ray diffraction, indicating the same packing motifs. Elucidated by the single-crystal X-ray analysis, the peaks observed in the out-of-plane XRD are indexed as (00*l*) planes for BOPAnt, (00*l*) planes for BSPAnt, and (*h*00) planes for BEPAnt, respectively, which indicates that the molecule crystallographic long axis is nearly perpendicular to the substrate surface. This is in fact a common feature for most high-performance (acene and thienoacene) organic semiconductors. XRD patterns of the thin films deposited on Si/SiO$_2$ substrates at 20 °C (RT) and 60 °C are shown in Fig. 4. As the substrate temperature increased, the XRD patterns showed higher order reflections, suggesting a better ordering in films grown at higher temperatures.[30]

Besides molecular packing, the mesoscale morphology can also impact device's performance. Fig. 5 shows the AFM images of three semiconductor films with a thickness of 40 nm deposited on Si/SiO$_2$ substrates at both 20 °C and 60 °C. We can see

Table 2 OTFT performance of diphenylanthracenes

	Thin film device				Modelling
SC	T_{sub} (°C)	Mobility (cm^2 V^{-1} s^{-1})	I_{on}/I_{off}	V_{th} (V)	Mobility (cm^2 V^{-1} s^{-1})
BOPAnt	20	0.76	6.1×10^6	−38.4	0.26
	60	2.96	1.1×10^5	−56.0	
BSPAnt	20	0.12	8.5×10^5	−45.6	0.11
	60	0.12	2.2×10^4	−52.7	
BEPAnt	20	1.49	1.2×10^5	−43.9	0.66
	60	3.72	1.3×10^6	−49.4	

dendrite growth in all materials at RT, but as the substrate temperature during the deposition T_{sub} is increased, the dendrites disappear in BEPAnt and BOPAnt and these films showed large grains with well-defined terraces. However, a three dimensional dendrite structure still dominated BSPAnt films grown at 60 °C. From cross-sectional analysis of the AFM image, the step height of BSPAnt terraces matches with the length of the molecule in an extended conformation, albeit with quite varieties. This is probably because of the very small domain sizes of BSPAnt. The observed small terrace islands may be due to the triclinic crystal packing of the BSPAnt molecule, where the individual grains in a polycrystalline films are not required to be arranged parallel to each other, similar to the triclinic crystal structure of pentacene molecules.[31] On the other hand, we can clearly see the step heights of the

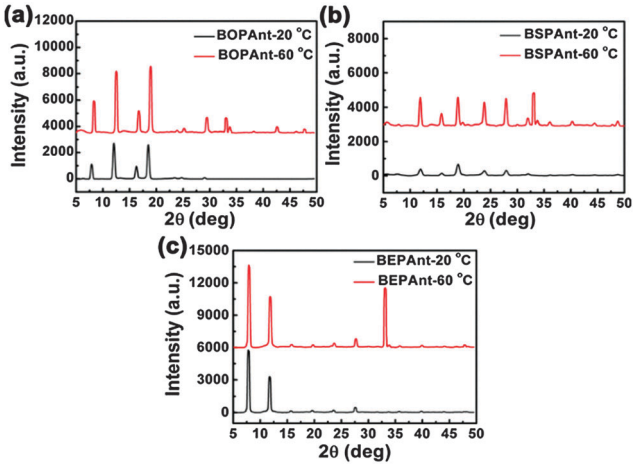

Fig. 4 XRD of the thin films ((a) BOPAnt, (b) BSPAnt, and (c) BEPAnt) deposited at 20 °C (black peaks) and at 60 °C (red peaks).

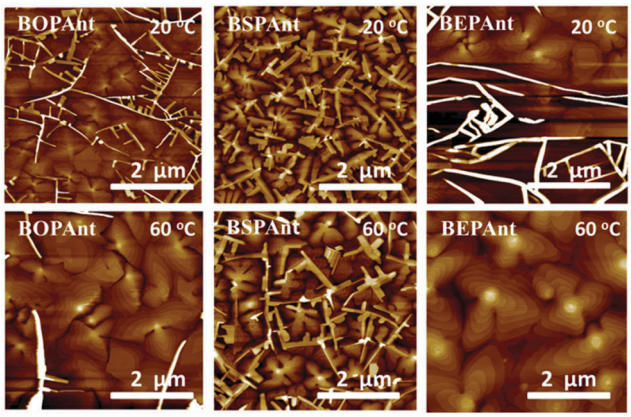

Fig. 5 AFM images of the thin films (from left to right: BOPAnt, BSPAnt, and BEPAnt, respectively) of the three semiconductor films deposited on the OTS-treated wafer substrate at both 20 °C (RT) and at 60 °C.

terraces in both BOPAnt and BEPAnt films and they are in good agreement with the extended molecular lengths of respective molecules, which indicates that the terraces are monomolecular layers. This means that the molecules of BOPAnt and BEPAnt are arranged normal to the substrate and the π–π interactions take place parallel to the substrate, which is a prerequisite for obtaining high carrier mobility in OTFT devices.[32,33] The orthorhombic crystal structure of BOPAnt and the monoclinic crystal structure of BEPAnt have preferred grain orientations in-plane and tend to possess vertical molecular arrangements owing to their 90° interaxial angles. In general, the average dendrite or grain size is increased as T_{sub} increases to 60 °C. The high mobility is attributed to the highly ordered crystal thin films. BEPAnt and BOPAnt films show very large grains with average size over 2 μm and thus the expected higher mobility is observed. The morphology of these polycrystalline films, as corroborated by AFM and XRD measurements, is likely the main factor explaining the differences of the charge mobility of corresponding OTFT devices. The same trend was further

Table 3 The DFT predicted hole and electron mobilities along the different molecular packing directions (in $cm^2 V^{-1} s^{-1}$)[a]

Compound	μ_h	μ_e	$\parallel\mu_h$	$\parallel\mu_e$	$\perp\mu_h$	$\perp\mu_e$
BOPAnt	0.263	1.714	0.234	1.714	0.881	0.000
BSPAnt	0.108	0.007	0.041	0.007	0.348	0.001
BEPAnt	0.658	1.259	0.658	1.260	0.002	0.001

[a] Total hole and electron mobilities (μ_h and μ_e); hole and electron mobilities parallel to the molecular axis ($\parallel\mu_h$ and $\parallel\mu_e$); hole and electron mobilities parallel to the molecular axis ($\perp\mu_h$ and $\perp\mu_e$).

confirmed by the molecule modelling study *via* DFT methods performed using the Gaussian 09 program. Based on the optimized single molecular structure configurations and the single crystal data molecular packing structures, the charge mobility data were predicted by using Marcus charge-transfer theory as listed in Table 2 for comparison.

The charge transport properties are associated with the molecule reorganization energy and the intermolecular electronic couplings. We analysed the heteroatom effects on the molecular reorganization energy. These calculated data are listed in (ESI†) Table S2 and Tables 2 and 3. The tables list the calculation data for both hole and electron reorganization energy levels and the respected hole and electron coupling data. As noted in Tables 2 and 3, the theoretical predicted mobilities for three compounds are in the same order as the experimental results. It should be noticed that BEPAnt shows two slightly different single crystal structures due to different orientations of its ethyl substituents (see Fig. S3, ESI†). Theoretical calculations show that the vertically aligned ethyl structure has higher hole and electron mobilities. Therefore, in the actual solid layer of the device the two different crystals should co-exist; the higher mobility was observed at higher deposition temperature, suggesting the increased content of vertically aligned ethyl form of the BEPAnt. The anisotropic properties of these molecules were also investigated by calculating the mobilities in both parallel and vertical packing directions. It seems the lowest mobility observed in BSPAnt is due to very low transfer integral in the parallel direction, highlighting the great impacts of the molecular packing on the charge mobilities of these heteroatom-modified anthracene derivatives.

The anisotropic transport properties of these compounds as suggested by the DFT predictions are listed in Table 3. The electron mobility along the molecular axis is very small (close to zero) with small electronic coupling. The high hole mobility in BEPAnt and BOPAnt was contributed mainly by the parallel packing of this compound with the highest $\parallel\mu_h$; these results are in good agreement with the experimental observations. For example, the mobility along the molecular long axis should be small (small electronic coupling). A similar trend has been predicated by other organic semiconductors.[34,35]

Conclusions

We have successfully synthesized three organic semiconductors by varying the heteroatoms. BEPAnt and BOPAnt demonstrated high charge mobility, with a thin-film transistor mobility over

3.72 cm^2 V^{-1} s^{-1}, making them among the best molecular semiconductors. All the semiconductors show high blue fluorescence properties. Noticeably, the heteroatoms (O, S) between the side chain and the aromatic ring can dramatically affect the charge mobility of the materials, besides the morphology of the deposited thin films, molecular packing, anisotropic mobility and the charge density. Our studies provide valuable information for future rational design of multifunctional electronic materials for advanced device applications.

Conflict of interest

The authors declare no competing financial interest.

Acknowledgements

The authors are thankful to Mr H. Zhang, Dr H. Dong, and Prof. W. Hu (Institute of Chemistry, Chinese Academy of Sciences) for discussion. This work is supported by Shenzhen Key Laboratory of Shenzhen Science and Technology Plan (ZDSYS20140509094114164), Guangdong Talents Project, NSFC (51373075), National Basic Research Program of China (973 Program, No. 2015CB856505; 2015CB932200), The National Research Foundation (20133221 110004), the Shenzhen Peacock Progra (KQTD2014062714543296), Provincial Science and technology project of Guangdong Province (2015B090914002; 2014B090914003).

Notes and references

1 M.-X. Zhang and G.-J. Zhao, *J. Phys. Chem. C*, 2012, **116**, 19197–19202.
2 J. Liu, B. Walker, A. Tamayo, Y. Zhang and T.-Q. Nguyen, *Adv. Funct. Mater.*, 2013, **23**, 47–56.
3 J. S. Kim, Z. Fei, S. Wood, D. T. James, M. Sim, K. Cho, M. J. Heeney and J.-S. Kim, *Adv. Energy Mater.*, 2014, **4**, 1400527.
4 G. R. Hutchison, M. A. Ratner and T. J. Marks, *J. Am. Chem. Soc.*, 2005, **127**, 16866–16881.
5 Y. Shirota and H. Kageyama, *Chem. Rev.*, 2007, **107**, 953–1010.
6 J. G. C. Veinot and T. J. Marks, *Acc. Chem. Res.*, 2005, **38**, 632–643.
7 J. Mei, Y. Diao, A. L. Appleton, L. Fang and Z. Bao, *J. Am. Chem. Soc.*, 2013, **135**, 6724–6746.
8 J. E. Coughlin, Z. B. Henson, G. C. Welch and G. C. Bazan, *Acc. Chem. Res.*, 2014, **47**, 257–270.
9 Y. Chen, X. Wan and G. Long, *Acc. Chem. Res.*, 2013, **46**, 2645–2655.
10 C. Melzer and H. von Seggern, *Nat. Mater.*, 2010, **9**, 470–472.
11 R. Capelli, S. Toffanin, G. Generali, H. Usta, A. Facchetti and M. Muccini, *Nat. Mater.*, 2010, **9**, 496–503.
12 G. Gelinck, P. Heremans, K. Nomoto and T. D. Anthopoulos, *Adv. Mater.*, 2010, **22**, 3778–3798.
13 Y. Diao, B. C. K. Tee, G. Giri, J. Xu, D. H. Kim, H. A. Becerril, R. M. Stoltenberg, T. H. Lee, G. Xue, S. C. B. Mannsfeld and Z. Bao, *Nat. Mater.*, 2013, **12**, 665–671.
14 A. Dadvand, A. G. Moiseev, K. Sawabe, W.-H. Sun, B. Djukic, I. Chung, T. Takenobu, F. Rosei and D. F. Perepichka, *Angew. Chem., Int. Ed.*, 2012, **51**, 3837–3841.
15 J. E. Anthony, *Angew. Chem., Int. Ed.*, 2008, **47**, 452–483.
16 A. Y. Amin, A. Khassanov, K. Reuter, T. Meyer-Friedrichsen and M. Halik, *J. Am. Chem. Soc.*, 2012, **134**, 16548–16550.
17 O. H. LeBlanc Jr, *J. Chem. Phys.*, 1961, **35**, 1275–1280.
18 J. Liu, H. Dong, Z. Wang, D. Ji, C. Cheng, H. Geng, H. Zhang, Y. Zhen, L. Jiang, H. Fu, Z. Bo, W. Chen, Z. Shuai and W. Hu, *Chem. Commun.*, 2015, **51**, 11777–11779.
19 J. Liu, H. Zhang and H. Dong, *et al.*, *Nat. Commun.*, 2015, **6**, 10032.
20 H. Meng, F. Sun, M. B. Goldfinger, G. D. Jaycox, Z. Li, W. J. Marshall and G. S. Blackman, *J. Am. Chem. Soc.*, 2005, **127**, 2406–2407.
21 H. Meng, M. Bendikov, G. Mitchell, R. Helgeson, F. Wudl, Z. Bao, T. Siegrist, C. Kloc and C. H. Chen, *Adv. Mater.*, 2003, **15**, 1090–1093.
22 B. Kan, Q. Zhang, M. Li, X. Wan, W. Ni, G. Long, Y. Wang, X. Yang, H. Feng and Y. Chen, *J. Am. Chem. Soc.*, 2014, **136**, 15529–15532.
23 K. Li, Z. Li, K. Feng, X. Xu, L. Wang and Q. Peng, *J. Am. Chem. Soc.*, 2013, **135**, 13549–13557.
24 V. Coropceanu, J. Cornil, D. A. da Silva Filho, Y. Olivier, R. Silbey and J.-L. Brédas, *Chem. Rev.*, 2007, **107**, 926–952.
25 T. Kimoto, K. Tanaka, M. Kawahata, K. Yamaguchi, S. Otsubo, Y. Sakai, Y. Ono, A. Ohno and K. Kobayashi, *J. Org. Chem.*, 2011, **76**, 5018–5025.
26 K. Kobayashi, H. Masu, A. Shuto and K. Yamaguchi, *Chem. Mater.*, 2005, **17**, 6666–6673.
27 C. M. Cardona, W. Li, A. E. Kaifer, D. Stockdale and G. C. Bazan, *Adv. Mater.*, 2011, **23**, 2367–2371.
28 H. Klauk, U. Zschieschang, R. T. Weitz, H. Meng, F. Sun, G. Nunes, D. E. Keys, C. R. Fincher and Z. Xiang, *Adv. Mater.*, 2007, **19**, 3882–3887.
29 (*a*) D. Kumaki, T. Umeda, T. Suzuki and S. Tokito, *Org. Electron.*, 2008, **9**, 921–924; (*b*) J. Soeda, Y. Hirose, M. Yamagishi, A. Nakao, T. Uemura, K. Nakayama, M. Uno, Y. Nakazawa, K. Takimiya and J. Takeya, *Adv. Mater.*, 2011, **23**, 3309–3314.
30 K. Takimiya, I. Osaka, T. Mori and M. Nakano, *Acc. Chem. Res.*, 2014, **47**, 1493–1502.
31 F. J. M. Zu Heringdorf, M. C. Reuter and R. M. Tromp, *Nature*, 2001, **412**, 517–520.
32 G. Witte and C. J. Wöll, *J. Mater. Res.*, 2004, **19**, 1889–1916.
33 H. Dong, X. Fu and J. Liu, *et al.*, *Adv. Mater.*, 2013, **25**, 6158–6183.
34 J. D. Huang, S. H. Wen, W. Q. Deng and K. L. Han, *J. Phys. Chem. B*, 2011, **115**, 2140–2147.
35 P. Li, Y. H. Cui, C. P. Song and H. Y. Zhang, *RSC Adv.*, 2015, **5**, 50212–50222.

